

**Fast and controlled fabrication of porous graphene oxide  
Application of AFM tapping for mechano-chemistry**

Chu, Liangyong; Korobko, Alexander V.; Bus, Marcel; Boshuizen, Bart; Sudhölter, Ernst J.R.; Besseling, Nicolaas A.M.

**DOI**

[10.1088/1361-6528/aaafc5](https://doi.org/10.1088/1361-6528/aaafc5)

**Publication date**

2018

**Document Version**

Final published version

**Published in**

Nanotechnology

**Citation (APA)**

Chu, L., Korobko, A. V., Bus, M., Boshuizen, B., Sudhölter, E. J. R., & Besseling, N. A. M. (2018). Fast and controlled fabrication of porous graphene oxide: Application of AFM tapping for mechano-chemistry. *Nanotechnology*, 29(18), 1-10. Article 185301. <https://doi.org/10.1088/1361-6528/aaafc5>

**Important note**

To cite this publication, please use the final published version (if applicable).  
Please check the document version above.

**Copyright**

Other than for strictly personal use, it is not permitted to download, forward or distribute the text or part of it, without the consent of the author(s) and/or copyright holder(s), unless the work is under an open content license such as Creative Commons.

**Takedown policy**

Please contact us and provide details if you believe this document breaches copyrights.  
We will remove access to the work immediately and investigate your claim.

PAPER

# Fast and controlled fabrication of porous graphene oxide: application of AFM tapping for mechano-chemistry

To cite this article: Liangyong Chu *et al* 2018 *Nanotechnology* **29** 185301

View the [article online](#) for updates and enhancements.

## Related content

- [Electrochemical performance of nitrogen and oxygen radio-frequency plasma induced functional groups on tri-layered reduced graphene oxide](#)  
J Lavanya, N Gomathi and S Neogi
- [Thermal scanning probe lithography for the directed self-assembly of block copolymers](#)  
S Gottlieb, M Lorenzoni, L Evangelio et al.
- [Direct growth of large-area graphene films onto oxygen plasma-etched quartz for nitrogen dioxide gas detection](#)  
H Yang, L Huang, Q H Chang et al.

# Fast and controlled fabrication of porous graphene oxide: application of AFM tapping for mechano-chemistry

Liangyong Chu<sup>1</sup> , Alexander V Korobko, Marcel Bus, Bart Boshuizen, Ernst J R Sudhölter and Nicolaas A M Besseling<sup>1</sup>

Chemical Engineering, Organic Materials & Interface (OMI), Delft University of Technology Van der Maasweg 9, 2629 HZ Delft, The Netherlands

E-mail: [L.Chu@tudelft.nl](mailto:L.Chu@tudelft.nl) and [klaas.besseling@gmail.com](mailto:klaas.besseling@gmail.com)

Received 17 November 2017, revised 5 February 2018

Accepted for publication 15 February 2018

Published 8 March 2018



CrossMark

## Abstract

This paper describes a novel method to fabricate porous graphene oxide (PGO) from GO by exposure to oxygen plasma. Compared to other methods to fabricate PGO described so far, e.g. the thermal and steam etching methods, oxygen plasma etching method is much faster. We studied the development of the porosity with exposure time using atomic force microscopy (AFM). It was found that the development of PGO upon oxygen-plasma exposure can be controlled by tapping mode AFM scanning using a Si tip. AFM tapping stalls the growth of pores upon further plasma exposure at a level that coincides with the fraction of  $sp^2$  carbons in the GO starting material. We suggest that AFM tapping procedure changes the bond structure of the intermediate PGO structure, and these stabilized PGO structures cannot be further etched by oxygen plasma. This constitutes the first report of tapping AFM as a tool for local mechano-chemistry.

Supplementary material for this article is available [online](#)

Keywords: porous network, graphene oxide, atomic force microscopy, oxygen plasma, mechano-chemistry

(Some figures may appear in colour only in the online journal)

## Introduction

2D materials, with extremely high aspect ratio and specific surface area, are promising for various applications, e.g. energy conversion and storage, sensors, composites, nano-mechanical and electrical devices [1, 2]. Creating pores in 2D materials has become an increasingly crucial topic in these applications [3–5], which include hydrogen storage [6], energy and fuel cells [7–12], molecular separation and ion recovery [13–19]. For graphene and its derivatives, which are the most popular 2D materials [20], chemical bottom-up approaches [21], hydro- or carbo-thermal etching of graphene oxide (GO) [22] and physical high-energy techniques [17, 23] are employed to fabricate porous 2D structures. Efficient

fabrication of 2D porous network structures by these methods knows many challenges that impede practical applications. For instance, the bottom-up approach and high energy techniques are complex and small-scale [17, 21, 23]. Thermal etching of GO, which is low-cost and large-scale [22, 24], is multi-step and time-consuming (from hours to several days) [22, 24]. As other compounds are used during the etching, post-etching purification and transfer of the products are also challenging [22, 24]. Moreover, among all these methods, tuning and control of the porous structure formation have not been reported so far.

GO comprises of graphene domains and more polar, hydroxylated ones [25–27]. When exposed to oxygen plasma, the different GO domains are etched with different rates [28, 29]. In this work we study the formation of porous GO (PGO) by oxygen-plasma etching of GO, deposited on Si

<sup>1</sup> Authors to whom any correspondence should be addressed.

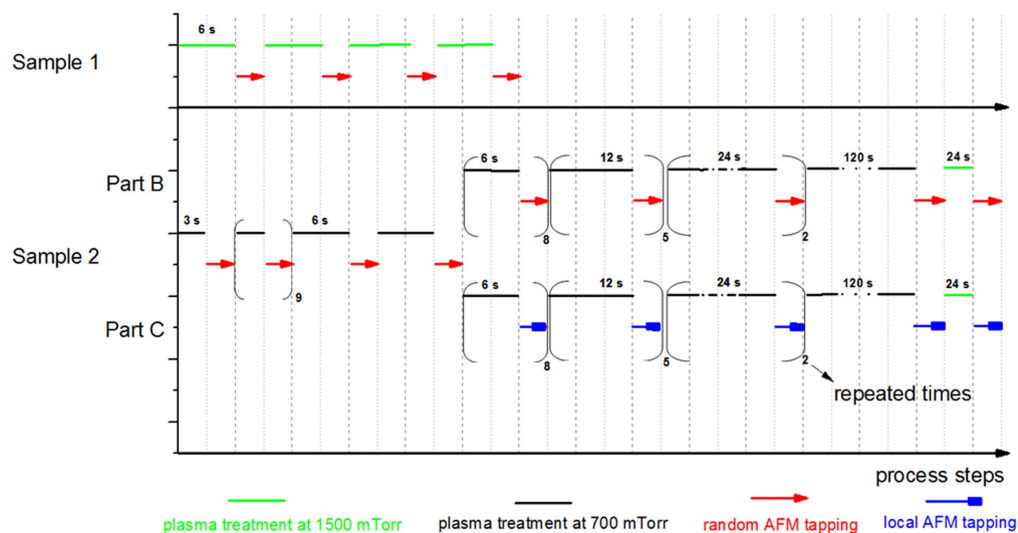


Figure 1. Samples sequential treatment.

wafer with an interlayer of polydiallyldimethylammonium (PDADMA). This interlayer strongly enhances the deposition of GO from an aqueous dispersion, because PDADMA is cationic, and GO anionic when the pH is about neutral or higher. We denote this layered system by GO/PDADMA/Si.

## Methods

### Chemicals and materials

Graphene oxide (GO), synthesized using Hummer's method, was purchased from Graphene Supermarket. The elemental composition of GO was characterized using x-ray photoelectron spectroscopy (XPS) [30]. A stable dispersion of 0.5 g GO in 1 l Milli-Q water was prepared using ultrasonication for 1 h (a USC-TH ultrasonic bath from VWR Scientific). The dispersion then was centrifuged at 4000 rpm for 1 h (Megafuge 2.0 R centrifuge from Heraeus Instruments, rotor radius of 20 cm). The supernatant was decanted and used for the sample preparation. Polydiallyldimethylammonium chloride (PDADMAC,  $M_w = 200\,000 \sim 350\,000 \text{ g mol}^{-1}$ , 20 wt% in water) solution and polyethylenimine (PEI,  $M_w = 25\,000 \text{ g mol}^{-1}$ ) were purchased from Sigma-Aldrich and used as received.  $0.1 \text{ g l}^{-1}$  aqueous polyelectrolyte solutions were prepared in milli-Q water. A chip of about of  $1 \text{ cm} \times 1 \text{ cm}$  was cut from a (100) Silicon wafer with a native oxide layer of about 2 nm obtained from Sil'Tronix Silicon Technologies. The silicon chip was firstly rinsed with demi-water and ethanol followed by sonication using ethanol and acetone for 5 min, respectively. Oxygen plasma treatments of a silicon chip were performed for 1 min at a pressure of 1600 mTorr, using a Harrick plasma cleaner (Anadis Instruments). After plasma treatment, the silicon chip was stored in Milli-Q water for at least 24 h to equilibrate.

### Sample preparation

Four different types of samples are prepared: GO/Si, hydrated and dried GO/PDADMAC/Si and dried GO/PEI/Si.

GO/PEI/Si and GO/PDADMA/Si samples were prepared by first coating the Si surface with a monolayer of polycations by dipping it in an aqueous PEI or PDADMAC solution ( $0.1 \text{ g l}^{-1}$ ) for 15 min. The sample was then rinsed with Milli-Q water for 5 min to remove non-adsorbed polyelectrolyte. After that, GO solutions were spin-coated onto the polycation/Si surfaces at 2000 rpm (IBIS spincoater from Intersens Instruments B.V.). Due to carboxylic groups, GO is negatively charged at about neutral pH, and adsorbs at the positively charged PEI or PDADMA layer. For GO/Si samples, GO solutions were directly spin-coated onto the Si surface, after which the sample was rinsed with Milli-Q water for 5 min to remove excess GO from the surface. To prepare the dried samples, they were kept in an oven for 3 h at  $70^\circ \text{C}$ . For obvious reasons, the GO coverage of GO/Si samples is much lower than for GO/PEI/Si and GO/PDADMA/Si samples. All the dipping steps were carried out whilst the solution was stirred.

For the oxygen plasma treatments of GO coated samples, we used the same instrument as with the cleaning of the silicon chips. The samples are put on a glass disk which has to be placed at the same position in the plasma chamber for each treatment. The details of sample preparations and measurements are summarized in figure 1. For example, the first GO/PDADMAC/Si sample (sample 1) was under oxygen plasma following the treatment sequence 6 s, 6 s, 6 s and 6 s (24 s in total) of at  $1500 \pm 100 \text{ mTorr}$ . The time for AFM measurements is arbitrary and varies from one sequence to another. To see the effect of AFM tapping on the plasma etching process, AFM measurements were performed on the same sample surface after each plasma treatment step (local AFM tapping) and on the sample surfaces randomly selected to avoid the scanning of the same area (random AFM tapping).

### AFM imaging

A SOLVER NEXT AFM instrument from NT-MDT was used in all AFM experiments. Tapping mode AFM measurements were done with a HA-NC silicon tip purchased from NT-MDT,

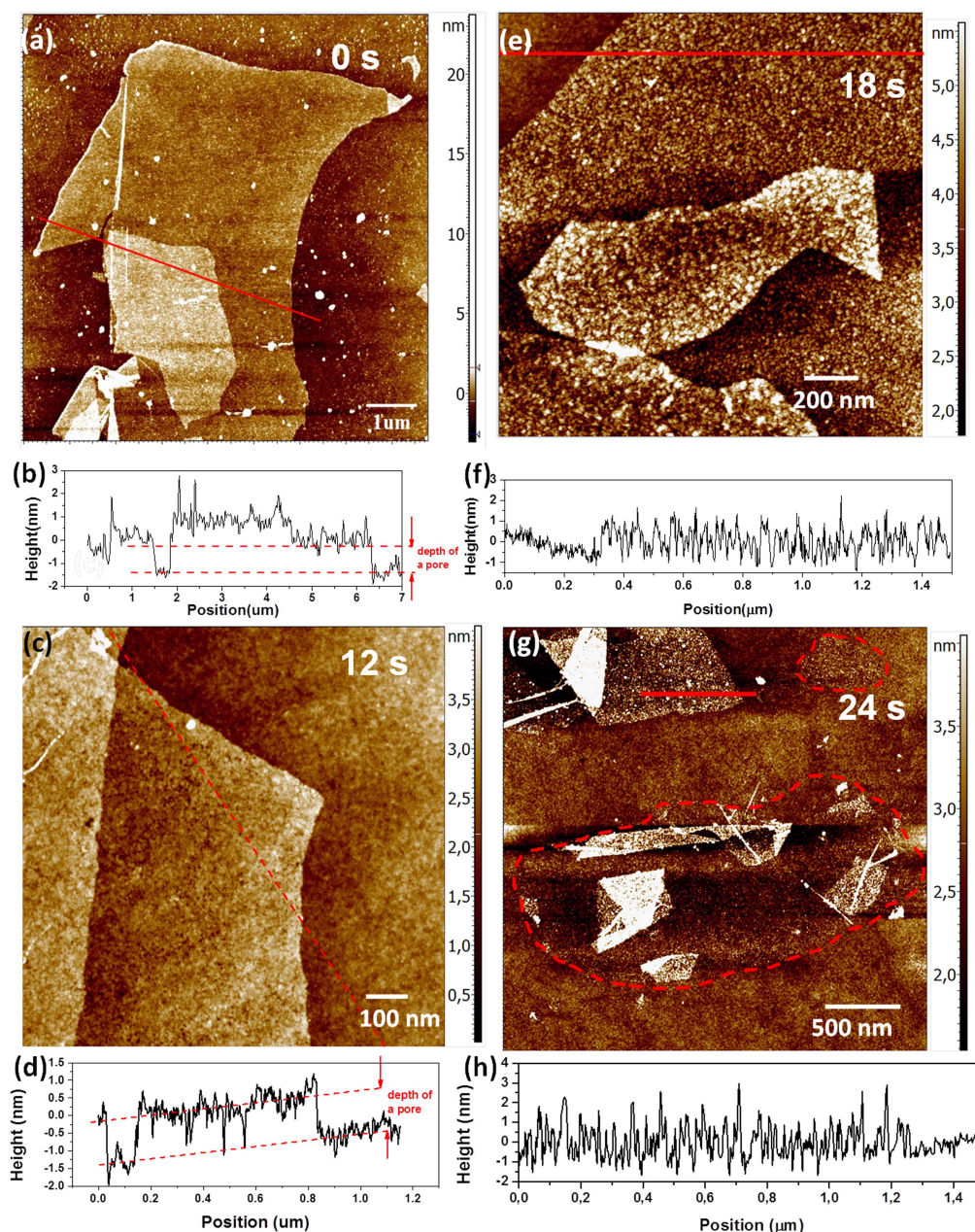


**Figure 2.** (a) AFM height image of an untreated GO/PDADMA/Si sample. (b) Height profile along the red line in (a). (c) AFM height image of a different region of the same sample as in (a), after treatment with oxygen plasma for 12 s in total at  $1500 \pm 100$  mTorr. A larger-area scan including this region is shown in figure S1(a) (supporting information). (d) Height profile along the red line in (c). (e) AFM height image of a different region of the same sample, after treatment with oxygen plasma for 18 s in total. (f) Height profile along the red line in (e). (g) AFM height image of again a different region of the same sample, after treatment with oxygen plasma for 24 s in total. The red dashed lines show the edges of the monolayer GO. The larger-area scan including this region is shown in figure S1(b). (h) Height profile along the red line in (g).

with a nominal value for the tip radius of 7 nm (guaranteed  $< 10$  nm). A sharp AFM tip (diamond-like carbon tip, with tip curvature radius of 1–3 nm) from NT-MDT was employed to characterize small holes in graphene oxide. Images obtained with the help of the sharp tip are explicitly indicated in the text and captions to figures below. In all other cases, a HA-NC tip was used. For the repeated tapping-mode AFM scanning at the same area,  $2000 \times 2000$  points images were obtained on the  $2 \mu\text{m} \times 2 \mu\text{m}$  surface area, using a tapping frequency of 0.5 Hz.

## Results and discssions

Figure 2 shows the tapping-mode AFM height images of a GO/PDADMA/Si sample, when treated with oxygen plasma at a pressure of  $1500 \pm 100$  mTorr for 0, 12 s, 18 s and 24 s, respectively. As shown in figures 2(a), (b), the thickness of single layer GO nano-sheet deposited on PDADMAC is  $1.5 \pm 0.3$  nm, which is consistent with the literature results [31, 32]. The thickness of GO deposited on top of GO/PDADMA/Si, forming a GO bilayer on top of the PDADMA,

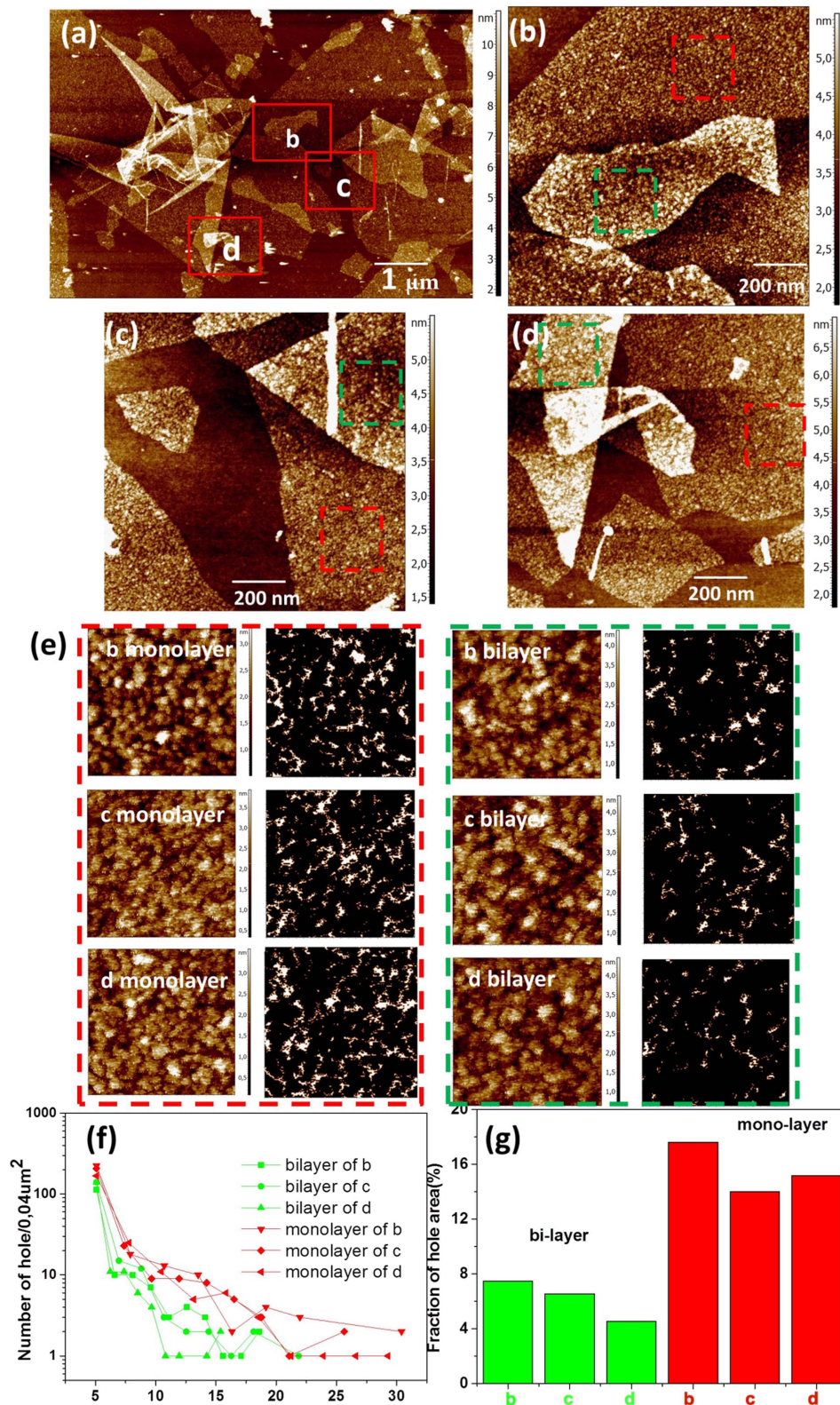


**Figure 3.** (a) AFM height image of GO/PDADMAC/Si. The sample is the same as in figure 2 after treatment with oxygen plasma for 18 s in total. Figures 2(b)–(d) show detailed AFM height images of areas denoted by the red boxes in (a) ((b), (c) and (d) respectively). The dashed red boxes in (b)–(d) mark monolayer GO and the dashed green boxes show bilayer GO. These areas ( $200 \times 200 \text{ nm}^2$ ) are studied quantitatively using the grain method. (e) The left images in the dashed red box are the selected monolayer areas and the right images show the porous structures (white corresponds to holes) revealed using the grain method. The dashed green box in (e) illustrates the grain method analysis for bilayer areas. (f) The pore-size distributions of the selected areas in (e). (g) The pore area in % of the total GO surface area shown in (e).

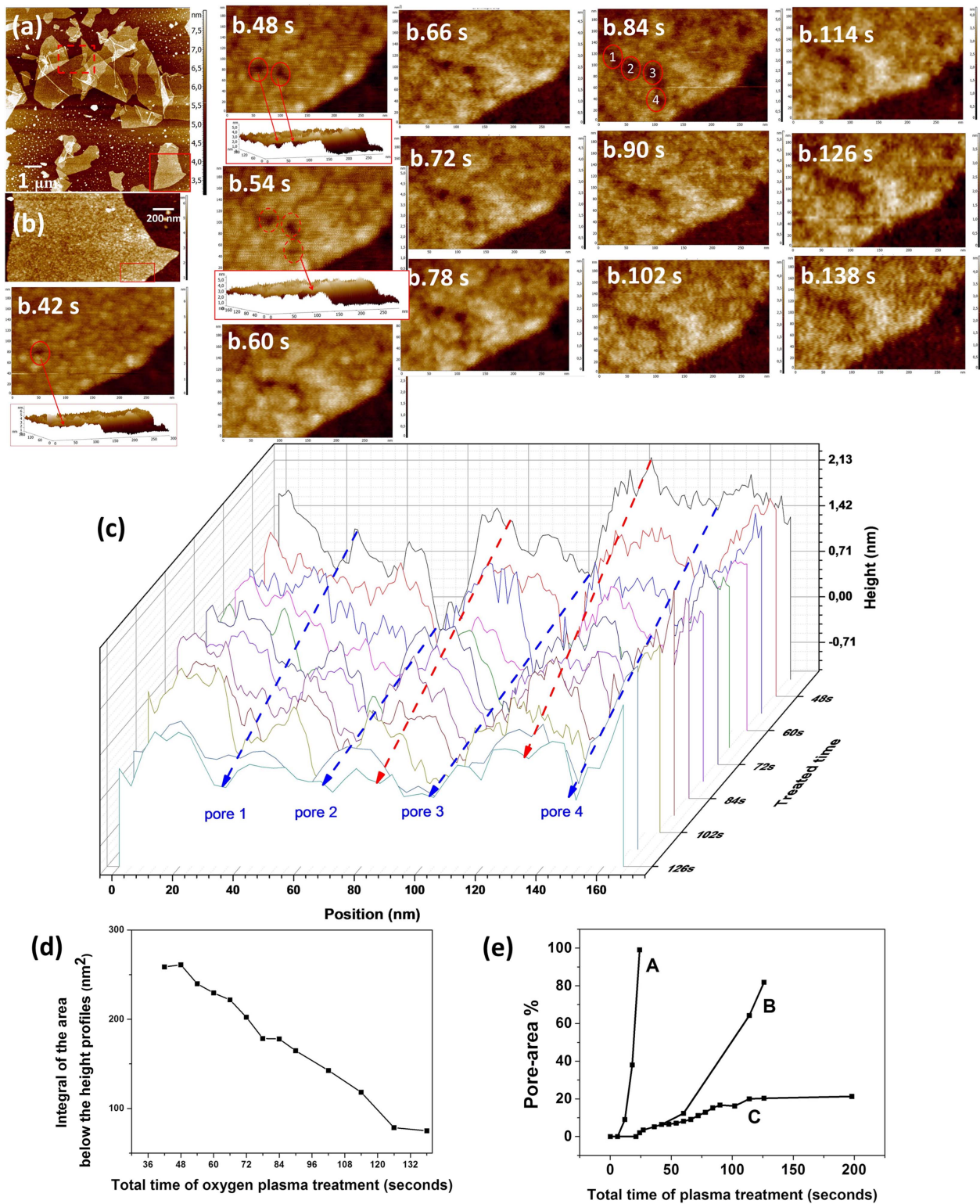


**Figure 4.** (a) Height morphology of a GO/PDADMA/Si sample treated for 42 s with oxygen plasma at 700 mTorr. (b) Detailed scan of the area marked by solid red box. Sequence of AFM images of the area enclosed by the red box of (b), recorded after each subsequent 6 s plasma treatment, named as b.42 s to b.138 s. In this area (200 × 300 nm<sup>2</sup>), 4 holes are formed as shown in b.84 s. (c) Height profiles taken along the line through the centers of each of four holes. (d) Integral of the area under the height profile lines in (c) versus plasma-exposure time. We assume that the depth of pore 2 is constant after 48 s treatment and the level at the bottom of that pore is chosen as the zero height level. (e) Development of the pore-area: the effect of plasma pressure and AFM tapping. The curves labeled A and B are for 1500 ± 100 mTorr and 700 mTorr, respectively. Each point of those dependencies corresponds to AFM measurements on randomly selected area of PGO. More data of AFM characterizations at 700 mTorr (curve B) are included in figure S6. The curve labeled C shows the stalling of pore growth at 700 mTorr for the area that undergoes repeated AFM tapping-mode imaging.

is slightly thinner (about  $1.0 \pm 0.3$  nm) than a first GO layer on top of PDADMA/Si [32]. So, a GO bilayer is thinner than twice a GO monolayer. It was found by others as well that a GO nano-sheet fits the roughness of another GO surface in contact better than with other surfaces [32]. Along the red line in figure 2(a), a rupture in the GO flake is clearly recognized, at the position  $1.5\text{--}1.8\ \mu\text{m}$  shown in figure 2(b). When the depth of a 'well' in a GO surface is comparable to that of the rift, the 'well' is assumed to completely perforate the GO layer, and denoted as a pore (see supporting information (2) is available online at [stacks.iop.org/NANO/29/185301/mmedia](http://stacks.iop.org/NANO/29/185301/mmedia)). The height profile in figure 2(b) shows that an untreated GO flake has a continuous 2D structure with a roughness of about 0.6 nm [32], and no pores are detected. After treatment with oxygen plasma for 3 s at  $1500 \pm 100$  mTorr, still no holes are visible (supporting information 3). This may however be due to the spatial resolution, which is dominated by the AFM-tip size. For AFM height-morphology scanning, the lateral resolution is largely determined by the radius of the AFM tip. The radius of the AFM tip used for most experiments was about 10 nm [30]. For 1 nm thick GO, only pores with a radius larger than 4.3 nm can be detected by the tip of this size (supporting information 4). Figure 2(c) shows the height morphology of the same sample, after another 9 s of plasma treatment at the same pressure (12 s in total). Pores are now clearly recognized as dark spots on the GO flakes. The height profile obtained along the dashed red line (see figure 2(c)) reveals a gap between two partly overlapping GO flakes at the position around  $0.1\ \mu\text{m}$ . We found that the depth of holes is similar to that of the gap, which confirms that the holes are indeed pores piercing the GO nano-sheets. The porosity of this PGO is quantified by analyzing the size distribution of the pores (supporting information 5) [33]. As shown in figure 2(e), after further plasma treatment for another 6 s (18 s in total), the number density of pores has significantly increased, both on the monolayer and bilayer patches. The holes start to connect with each other, forming larger holes. Figure 2(g) reflects the height morphology of the sample after further treatment with oxygen plasma at the same pressure for another 6 s (24 s in total). The dashed red lines indicate the circumferences of areas of monolayer GO. We can clearly see that the monolayer GO flakes in these areas are largely etched away. The bilayer patches still partially remain (figure 2(h)) and form a similar porous network structure as the monolayer PGO after 18 s of plasma treatment (supporting information 1).

As it is important for many applications to control the porosity of 2D materials, the pore-size distribution was analyzed after the sample had been treated with oxygen plasma for 18 s in total (figure 3). Figure 3(a) shows a large area of the sample, where several PGO flakes are clearly recognizable. We can distinguish between monolayer PGO and regions covered by two layers of PGO. In figure 3(e), enclosed by the dashed red box, three zoomed-in images of monolayer PGO are shown. Images of bilayer PGO are enclosed by the dashed green box. The pore-size distributions, obtained using the grain method [33], reveal that the number densities of small pores ( $O(5\ \text{nm})$ ) are similar for monolayer GO and for those GO that forms the top layer of a GO bilayer. However, larger pores are considerably more

numerous for monolayer GO. This indicates that the substrate below a GO flake influences its sensitivity to oxygen-plasma etching. GO deposited on PDADMA/Si is more sensitive to oxygen plasma than GO deposited on top of another GO layer. This is probably related to the finding that binding a GO sheet to other GO sheets is better than to substrates. The pore-size distributions of different PGO regions at the same substrate are roughly the same and small variations among the regions might be due to slight variations in the chemical composition of GO.

In order to quantify the evolution of PGO under oxygen plasma treatment, a new GO/PDADMAC/Si sample was prepared (see methods) and treated with plasma at 700 mTorr. The etching rate at 700 mTorr is expected to be slower than at higher plasma pressure, enabling us to better follow the time evolution of the pores. Using an ultra-sharp AFM tip (a diamond-like carbon tip, with tip curvature radius of  $1\text{--}3$  nm) and 700 mTorr oxygen plasma, pores with radii of  $2\text{--}5$  nm appear after the treatment time of sample exceeds 24 s, as shown in figures S6(b) and (c). No pores have been detected before that time (supporting information 7).

After plasma treatment at 700 mTorr for 42 s, holes are clearly visible in the AFM images (using the normal tip), figures 4(a) and (b). The area enclosed by a red box in figure 4(a) was investigated in more detail. After each subsequent 6 s plasma treatment, a height image was recorded by tapping mode AFM. The sequence of images illustrates the emergence, growth and clustering of holes (labeled 1–4 in the b.84 s image). These four holes gradually get connected and finally form single hole of larger size. Height profiles along a line through the centers of these four holes are shown in figure 4(c). Figure 4(d) shows the evolution of the integral of the area under the height profiles indicated in figure 4(c). This integral corresponds to the amount of material that is still left in the PGO sheet. We observe a linear decrease, which indicates the constant etching rate during the plasma treatment. At other positions, where no holes were formed after the first 42 s, no new holes are formed later on, and there is no material loss upon plasma exposure. These observations indicate GO has domains that are susceptible to oxygen plasma, where holes arise already after brief plasma exposure and domains that are more stable to the plasma treatment, where no holes appear even after prolonged exposure to the plasma.

Based on investigations described above, a region on a GO flake (the area enclosed by the red box in figure 4(a)) was repeatedly scanned by tapping-mode AFM after each short-time explosion of GO to the plasma. AFM data indicates that AFM tapping itself influences the evolution of the hole morphology upon plasma exposure. In order to prove this, we investigated the morphology of PGO surface after different durations of plasma exposure and at randomly selected locations, that had not been imaged before. Comparing the results of the latter measurement with those of the repeated measurements at the same area after each explosion to plasma, experimental observations clearly demonstrate that AFM tapping significantly influences the etching process. As figure 4(e) shows (and also figure S6), the etching rate of the PGO surface scanned by AFM after each short-term exposure to plasma was significantly lower (dependency C). Especially

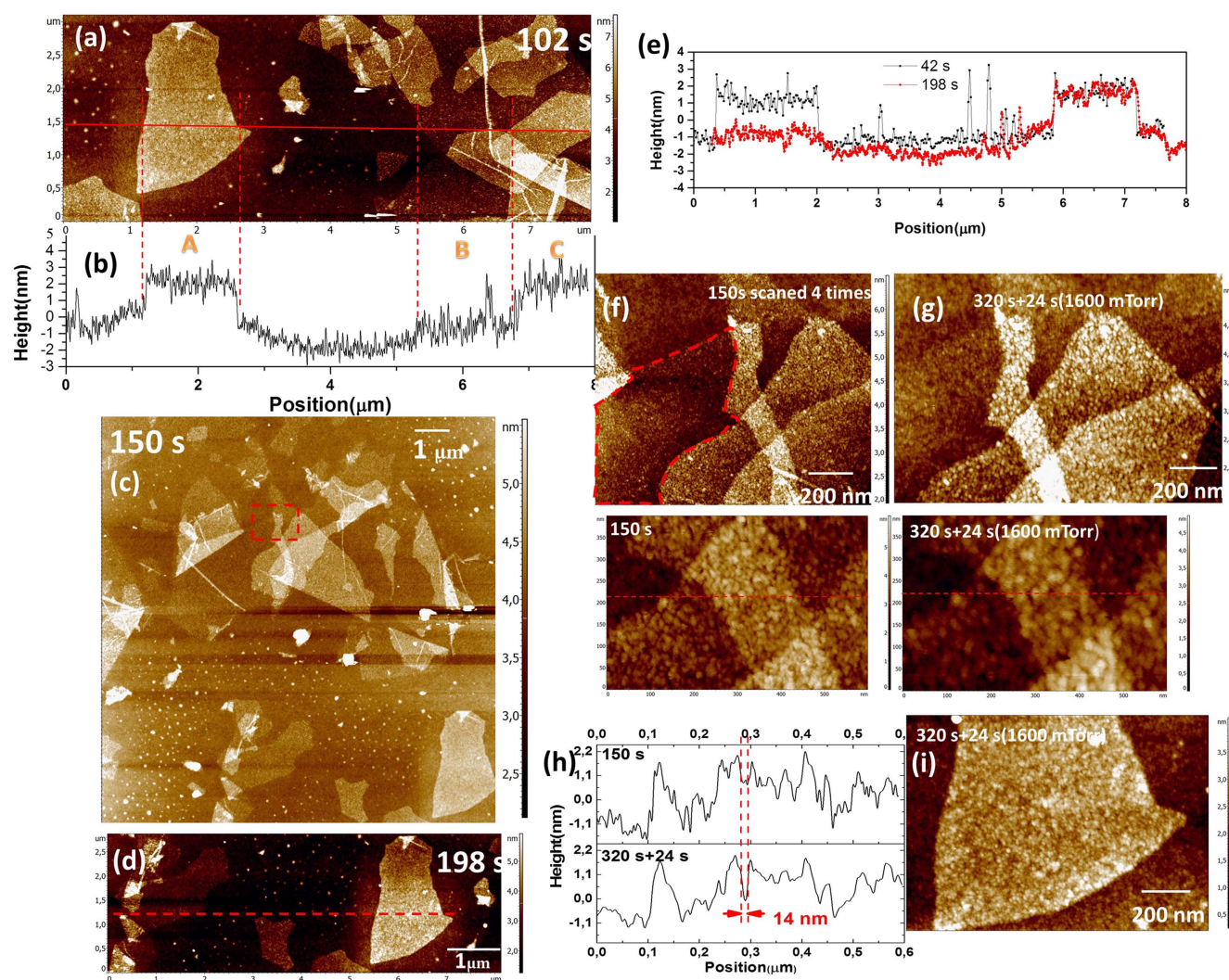


**Figure 5.** (a) Height morphology of the sample treated with oxygen plasma for 102 s at 700 mTorr. (b) Height profile along the red line in (a). (c) Height morphology of the sample treated with oxygen plasma for 150 s at 700 mTorr. The area is the same as in figure 5(a). (d) Height morphology of the sample treated with oxygen plasma for 198 s at 700 mTorr. (e) Height profiles along the dashed red line in (d) after 42 s and 198 s, respectively. (f) Detailed scans of the area enclosed by the dashed red box of (c) after 150 s of plasma treatment (in total). (g) Height profiles of the same area as (f), after 320 s of plasma treatment (in total) at 700 mTorr followed by an additional 24 s at  $1500 \pm 100$  mTorr. (h) Height profiles along the red line in (f) and (g). (i) Height profiles after the same treatments as with (g) of the area, where AFM imaging was performed after every plasma treatment. This demonstrates that the fabrication of PGO can be controlled by AFM tapping and patches with various porosities can be fabricated on the single PGO sheet.

after about 50 s, when the pore development started to level off (the red-boxed area, figure 4(a)). After about 120 s of plasma treatment with intermittent tapping-mode AFM scans, further pore development has ceased completely, and the total pore area reaches a plateau at high number of AFM scans.

In figures 5(a) and (b), we show the sample measured after 102 s of plasma treatment (see also figure 4(a), area noticed by the red box). The area belonging to interval A of the single scan was repeatedly scanned by tapping-mode AFM. Interval B, which runs across another GO monolayer (a long wrinkle is clearly recognized), was scanned for the first time when image 5(a) was obtained. We clearly observe that GO has eroded much more at B than at A. In fact, at B it is almost completely etched away. As shown in figures 5(d) and (e), after 198 s of plasma treatment, the GO that was repeatedly scanned by tapping-mode AFM is still largely

preserved, while the surrounding GO is almost completely etched away. So, it turns out that tapping mode AFM influences the evolution of PGO upon oxygen-plasma exposure, and that AFM tapping protects PGO against the effect of oxygen plasma. This implies that we can use AFM tapping as a tool for localized control of the porosity of PGO. In order to verify this, we made some further tests on the sample that had been treated with oxygen plasma at 700 mTorr for 150 s. We scanned the area (the same area enclosed by the dashed red box in figures 5(c) and 3(a)) for 4 times. We found that after these 150 s of plasma exposure, the monolayer PGO in this area (enclosed by a dashed red contour in figure 5(f)) is almost completely removed, similarly as for the other areas, shown in figures S6.2.g and S6.2.h Then the sample is further treated with oxygen plasma for another 120 s under 700 mTorr and 24 s at  $1500 \pm 100$  mTorr. AFM scanning shows that the area

under investigation does not change significantly after every plasma treatment as compared to what is seen in figure 5(i) and in the dashed red box in figure 5(c). The morphology of this area is similar to that of figure 5(h), which was obtained after 150 s of treatment.

We will now try to formulate a comprehensive interpretation of the observations described above: the generation and growth of holes in GO due to oxygen plasma, and the effect of AFM tapping on these processes. This interpretation is schematically illustrated in figure 6. First, we need to consider that GO has graphene domains and more polar hydroxylated domains. It is known that apolar compounds and moieties are more sensitive to oxygen-plasma than polar ones [34, 35]. We performed XPS measurements on original GO/PDADMAC/Si sample and on the GO/PDADMAC/Si sample treated by oxygen plasma for 18 s (at  $1500 \pm 100$  mTorr). XPS shows that after 18 s of plasma treatment, the ratio of C–C, C=C and C=O, C–O decreased from 0.731:1 to 0.601:1 (see supporting information 10). This indicates that carbon patches are firstly etched. For GO, this implies that the graphene domains are more sensitive to oxygen plasma than the hydroxylated ones, as the latter are less sensitive to oxygen ions due to the polar moieties. So, holes arising in the early stages of plasma treatment are formed most likely in the graphene domains, as illustrated in figure 6(1). Upon prolonged exposure to oxygen plasma, more holes are formed, most likely in the graphene domains, and existing holes grow larger in size. When the edge of a hole in a graphene domain reaches the boundary between the graphene and a hydroxylated domain, the hole can grow further because at the edge of a hole the backbone carbons of the hydroxylated domains are exposed to attack by high-energy oxygen species. So ultimately GO is completely etched away, as illustrated in the sequence 1–6 in figure 6. This corresponds to the experimental observations shown in figures 1(a)–(d), where we see the increase of holes both in numbers and in size, and for the region B in figures 6(a) and (b), where GO is almost completely etched away upon prolonged plasma treatment. This unbounded etching is quantified in curves A and B in figure 3(e). However, we observe (figure 3) that this does not happen for GO that is repeatedly scanned by tapping mode AFM. These images show that expansion of holes does not occur equally in all directions. Some holes become long and narrow rather than spherical. Moreover, the total hole area does not increase until all GO is etched away. Rather, the increase of the total hole area levels off and reaches a plateau, as quantified by curve C in figure 4(e). How to explain what is going on? A clue is offered by the finding that the total hole area of GO that undergoes repeated AFM tapping reaches a plateau at about 20% of the total area. This percentage corresponds to the percentage of  $sp^2$  hybridized carbon atoms in the GO starting material, as found by XPS [17]. Obviously,  $sp^2$  hybridized carbons correspond to graphene domains, whereas  $sp^3$  hybridized carbons correspond to the hydroxylated ones in the polar domains of GO. Hence, we infer that in some way AFM

tapping has the effect that hole growth beyond the graphene domains is prevented, and that the sizes and shapes of the holes, as obtained by the combination of plasma treatment and AFM tapping, correspond to the sizes and shapes of the graphene domains in the original GO starting material. This is illustrated in figures 6(2) and (3). It is still puzzling how AFM tapping brings about the effect of stabilizing the edges of hydroxylated domains and leads to protection against further attack by high-energy oxygen species. As the first step of etching at the atomistic level, high-energy oxygen species attach and form intermediate structures. Subsequently, C–C bonds break and small volatile molecules like CO, CO<sub>2</sub> detach. It seems that in some way the latter step is prevented by AFM tapping. In order to obtain an AFM image, the sample is taken out of the plasma chamber. This allows for the exposed C atoms and their dangling bonds to bond with water molecules from the air. These intermediate structures decrease the etching rate. This explains our finding that the etching rate we observed at 700 mTorr is significantly slower than 7/15 of that of at  $1500 \pm 100$  mTorr because with the lower pressure treatment the sample was taken out of the plasma chamber more often. This slows down but does not prevent further plasma etching. Only at regions that undergo AFM tapping, etching levels off and reaches a plateau value. Apparently, at those regions, intermediate polar moieties at the edges of hydroxylated domains are stabilized by AFM tapping. The edges of PGO are all covered by polar moieties, such as –OH, –O–, and –COOH groups. In this way, it leads to protection against further plasma etching (24 s at  $1500 \pm 100$  mTorr; figures 6(g) and (i)). This is illustrated in figures 6(3') and (4'). This effect of AFM tapping is an interesting example of mechano-chemistry [36], and it constitutes the first example of AFM tapping as a tool for local mechano-chemistry. Another interesting feature of the observed mechano-chemical effect observed here is that it involves stabilization of chemical structures, whereas most other known mechano-chemical effects involve breaking of, often macromolecular, bonds. Meanwhile, our observations constitute a warning that tapping-mode AFM imaging is not always as inconsequential for the investigated surfaces as is usually assumed.

According to the mechanism described above, the size and shape of the holes after plasma treatment in combination with AFM tapping correspond to those of the graphene domains of the GO starting material, as illustrated by figure 6(3') evolving from figure 6(0).

In practical applications, GO nanosheets are deposited on various substrates. Therefore, we briefly examined oxygen plasma etching of GO deposited on some other substrates: on silicon coated with another polycation (polyethyleneimine, PEI) and on silicon coated by its native oxide layer. We found that, after oxygen plasma treatment at  $1500 \pm 100$  mTorr for 12 s, pores in GO are found with all the samples. The AFM height morphologies of these plasma treated samples are shown in the supporting information, part 11. The growth rate was found to depend on the substrate.

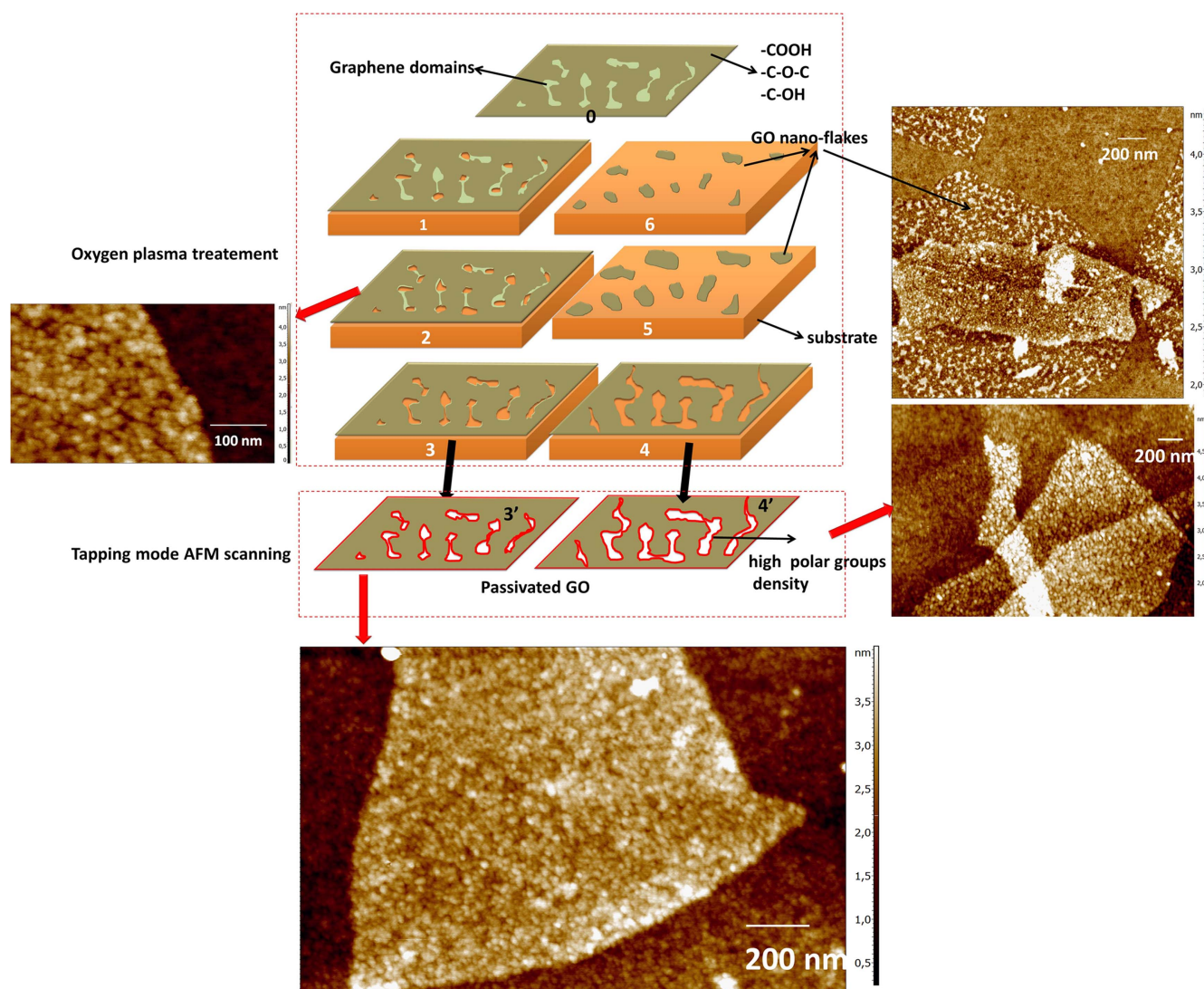


**Figure 6.** Schematic drawing of the evolution of PGO upon treatment by oxygen plasma and AFM tapping. Picture 0 shows the structure of GO, composed of graphene and hydroxylated domains. Structures 1–6 illustrate the evolution of PGO under oxygen plasma treatment. Initially (structures 0–2), C atoms of the graphene domains, that are directly exposed to oxygen plasma, are etched away. As the edge of a pore in a graphene domain reaches the border with a hydroxylated domain, C atoms of the hydroxylated domain at the edges of the pore get directly exposed to oxygen plasma. When the sample is not treated with AFM tapping, the etching at the edges of the holes can carry on into the graphene domains. As the holes get more and more connected, small GO flakes appear, which decrease in size upon further plasma treatment, as illustrated in structures 4–6. However, when the sample is treated by AFM tapping, the structure of the edges of the holes stabilize, and the holes do not grow beyond the graphene domains, as illustrated in 3' and 4'.

## Conclusions

We report a fast and controlled method to fabricate PGO and GO nano-flakes. PGO has a structure analogous to single layer covalent organic frameworks, and GO nano-flakes are promising to fabricate 2D quantum dots. GO comprises of graphene domains and more polar, hydroxylated ones. When exposed to oxygen plasma, the different GO domains are etched with different rates. Compared to other methods of fabricating PGO, the oxygen plasma etching method shows much promise in producing the porous 2D GO significantly faster. The porosity development with exposure time is studied with AFM. We demonstrate an effective approach to control the process of etching by applying AFM tapping in

between subsequent plasma treatments. We explain our result as following: AFM tapping changes the bond structure of the intermediate PGO structure and these stabilized PGO structure cannot be further etched by oxygen plasma. This constitutes the first example where AFM is applied as a tool for mechano-chemistry.

## Acknowledgments

We acknowledge the PhD Scholarship of Liangyong Chu from China Scholarship Council of the Ministry of Education of China (201306450011).

## Notes

The authors declare no competing financial interest.

## ORCID iDs

Liangyong Chu  <https://orcid.org/0000-0001-7496-4775>

## References

- [1] Gupta A, Sakhivel T and Seal S 2015 Recent development in 2D materials beyond graphene *Prog. Mater. Sci.* **73** 44
- [2] Xia F, Wang H, Xiao D, Dubey M and Ramasubramanian A 2014 Two-dimensional material nanophotonics *Nat. Photon.* **8** 899
- [3] Han S, Wu D, Li S, Zhang F and Feng X 2014 Porous graphene materials for advanced electrochemical energy storage and conversion devices *Adv. Mater.* **26** 849
- [4] Su C, Acik M, Takai K, Lu J, Hao S-J, Zheng Y, Wu P, Bao Q, Enoki T and Chabal Y J 2012 Probing the catalytic activity of porous graphene oxide and the origin of this behaviour *Nat. Commun.* **3** 1298
- [5] Zhang H, Hussain I, Brust M, Butler M F, Rannard S P and Cooper A I 2005 Aligned two- and three-dimensional structures by directional freezing of polymers and nanoparticles *Nat. Mater.* **4** 787
- [6] Du A, Zhu Z and Smith S C 2010 Multifunctional porous graphene for nanoelectronics and hydrogen storage: new properties revealed by first principle calculations *J. Am. Chem. Soc.* **132** 2876
- [7] Boutillier M S, Hadjiconstantinou N G and Karnik R 2017 Knudsen effusion through polymer-coated three-layer porous graphene membranes *Nanotechnology* **28** 184003
- [8] Etacheri V, Yourey J E and Bartlett B M 2014 Chemically bonded TiO<sub>2</sub>-bronze nanosheet/reduced graphene oxide hybrid for high-power lithium ion batteries *ACS Nano* **8** 1491
- [9] He J, Chen Y, Lv W, Wen K, Wang Z, Zhang W, Li Y, Qin W and He W 2016 Three-dimensional hierarchical reduced graphene oxide/tellurium nanowires: a high-performance freestanding cathode for Li-Te batteries *ACS Nano* **10** 8837
- [10] He J, Chen Y, Lv W, Wen K, Xu C, Zhang W, Qin W and He W 2016 Three-dimensional CNT/graphene-Li<sub>2</sub>S aerogel as freestanding cathode for high-performance Li-S batteries *ACS Energy Lett.* **1** 820
- [11] Lv W, Shi X, Huang H, Niu Y, Yang W, Liu P, Qin W and He W 2017 High O/C ratio graphene oxide anode for improved cyclic performance of lithium ion batteries and the in-operando Raman investigation of its (de) lithiation *Mater. Today Energy* **3** 40
- [12] Zhu Y, Murali S, Stoller M D, Ganesh K, Cai W, Ferreira P J, Pirkle A, Wallace R M, Cychosz K A and Thommes M 2011 Carbon-based supercapacitors produced by activation of graphene *Science* **332** 1537
- [13] Blankenburg S, Bieri M, Fasel R, Müllen K, Pignedoli C A and Passerone D 2010 Porous graphene as an atmospheric nanofilter *Small* **6** 2266
- [14] Huang K, Liu G, Lou Y, Dong Z, Shen J and Jin W 2014 A graphene oxide membrane with highly selective molecular separation of aqueous organic solution *Angew. Chem., Int. Ed. Engl.* **53** 6929
- [15] Jiang D-E, Cooper V R and Dai S 2009 Porous graphene as the ultimate membrane for gas separation *Nano Lett.* **9** 4019
- [16] Kim H W, Yoon H W, Yoon S-M, Yoo B M, Ahn B K, Cho Y H, Shin H J, Yang H, Paik U and Kwon S 2013 Selective gas transport through few-layered graphene and graphene oxide membranes *Science* **342** 91
- [17] Koenig S P, Wang L, Pellegrino J and Bunch J S 2012 Selective molecular sieving through porous graphene *Nat. Nanotechnol.* **7** 728
- [18] Shan M, Xue Q, Jing N, Ling C, Zhang T, Yan Z and Zheng J 2012 Influence of chemical functionalization on the CO<sub>2</sub>/N<sub>2</sub> separation performance of porous graphene membranes *Nanoscale* **4** 5477
- [19] Xu L, Zhou X, Tian W Q, Gao T, Zhang Y F, Lei S and Liu Z F 2014 Surface-confined single-layer covalent organic framework on single-layer graphene grown on copper foil *Angew. Chem., Int. Ed. Engl.* **53** 9564
- [20] Geim A K and Novoselov K S 2007 The rise of graphene *Nat. Mater.* **6** 183
- [21] Bieri M, Treier M, Cai J, Ait-Mansour K, Ruffieux P, Gröning O, Gröning P, Kastler M, Rieger R and Feng X 2009 Porous graphenes: two-dimensional polymer synthesis with atomic precision *Chem. Commun.* **45** 6919
- [22] Zhou D, Cui Y, Xiao P-W, Jiang M-Y and Han B-H 2014 A general and scalable synthesis approach to porous graphene *Nat. Commun.* **5** 4716
- [23] Zan R, Ramasse Q M, Bangert U and Novoselov K S 2012 Graphene reknits its holes *Nano Lett.* **12** 3936
- [24] Han T H, Huang Y-K, Tan A T, Dravid V P and Huang J 2011 Steam etched porous graphene oxide network for chemical sensing *J. Am. Chem. Soc.* **133** 15264
- [25] Erickson K, Emi R, Lee Z, Alem N, Gannett W and Zettl A 2010 Determination of the local chemical structure of graphene oxide and reduced graphene oxide *Adv. Mater.* **22** 4467
- [26] Kim J, Cote L J and Huang J 2012 Two-dimensional soft material: new faces of graphene oxide *Acc. Chem. Res.* **45** 1356
- [27] Pei S and Cheng H-M 2012 The reduction of graphene oxide *Carbon* **50** 3210
- [28] Felten A, Eckmann A, Pireaux J, Krupke R and Casiraghi C 2013 Controlled modification of mono- and bilayer graphene in O<sub>2</sub>, H<sub>2</sub> and CF<sub>4</sub> plasmas *Nanotechnology* **24** 355705
- [29] Gokus T, Nair R, Bonetti A, Böhm M, Lombardo A, Novoselov K, Geim A, Ferrari A and Hartschuh A 2009 Making graphene luminescent by oxygen plasma treatment *ACS Nano* **3** 3963
- [30] Chu L, Korobko A V, Cao A, Sachdeva S, Liu Z, de Smet L C, Sudhölter E J, Picken S J and Besseling N A 2016 Mimicking an atomically thin 'vacuum spacer' to measure the Hamaker constant between graphene oxide and silica *Adv. Mater. Interfaces* **4** 1600495
- [31] Dreyer D R, Park S, Bielawski C W and Ruoff R S 2010 The chemistry of graphene oxide *Chem. Soc. Rev.* **39** 228
- [32] Mkhoyan K A, Contryman A W, Silcox J, Stewart D A, Eda G, Mattevi C, Miller S and Chhowalla M 2009 Atomic and electronic structure of graphene-oxide *Nano Lett.* **9** 1058
- [33] Guan Q, Norder B, Chu L, Besseling N A, Picken S J and Dingemans T J 2016 All-aromatic (AB) n-multiblock copolymers via simple one-step melt condensation chemistry *Macromolecules* **49** 8549
- [34] Egitto F, Emmi F, Horwath R and Vukanovic V 1985 Plasma etching of organic materials: I. Polyimide in O<sub>2</sub>-CF<sub>4</sub> *J. Vac. Sci. Technol. B* **3** 893
- [35] Taylor G and Wolf T 1980 Oxygen plasma removal of thin polymer films *Polym. Eng. Sci.* **20** 1087
- [36] Hickenboth C R, Moore J S, White S R, Sottos N R, Baudry J and Wilson S R 2007 Biasing reaction pathways with mechanical force *Nature* **446** 423